

# Noise Decrease in a Balanced Self-Mixing Interferometer: Theory and Experiments

Parisa Esmaili<sup>1</sup>, Michele Norgia<sup>1</sup>, *Senior Member, IEEE*, and Silvano Donati<sup>2</sup>, *Life Fellow, IEEE*

**Abstract**—In a self-mixing interferometer built around a laser diode, the signals at the outputs of the two mirrors are in phase opposition, whereas noise fluctuations are partially correlated. Thus, on making the difference between the two outputs, the useful signal is doubled in amplitude and the signal-to-noise ratio is even more enhanced. Through a second-quantization model, the improvement is theoretically predicted to be dependent on laser facets reflectivity. The results are then validated by experimental measurements with different laser types that show very good agreement with theoretical results. The new technique is applicable to a number of already existent self-mixing sensors, potentially improving significantly their measurement performances.

**Index Terms**—Measurements, noise measurements, optical feedback, optical interferometers, semiconductor laser diodes (LDs).

## I. INTRODUCTION

SELF-MIXING interferometry (SMI) is a well-known configuration of interferometry that supplies, even without any optics external to the laser, amplitude modulation (AM) and frequency modulation (FM) [1], [2], [3], [4], just the ones necessary for unambiguous phase measurement. As a coherent process, SMI can work even with very low returning power (e.g.,  $10^{-8}$  of laser power), an attractive feature that has triggered many measurement applications in the fields, e.g., of mechanical metrology [5], for displacement [6], [7], [8], [9], [10], [11], [12], distance [13], [14], [15], [16], vibration [17], [18], [19], [20], and flow [21], [22], [23] measurement, with direct application also to biomedical signal sensing [24], [25], [26].

To access the AM self-mixing signal, it is customary to use the internal monitor photodiode, usually mounted in front of the rear mirror. We can process the AM signal either digital or analog, respectively, by fringes counting for measuring displacement up to several meters or by measuring vibrations taking advantage of the signal linearity, down to 100 pm and even much less with appropriate processing [2], [3]. Recently, the FM SMI signal was explored for sensing, showing a signal-to-noise ratio (SNR) improvement of about two orders of

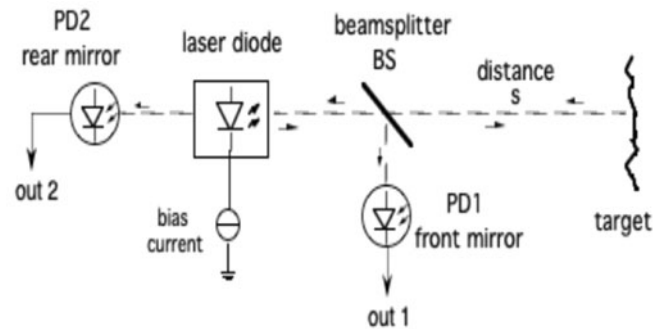


Fig. 1. Output signal from an SMI is measured at the rear mirror at PD2 and at the front mirror with the BS and PD1 combination.

magnitude with respect to AM [27], [28], [29], [30], but it requires a more complex and expensive optical setup. The aim of this work is to propose an improvement in traditional AM SMI signal detection, while keeping the absolute simplicity of the optical setup and potential low cost of the sensor.

As the SMI signal is a modulation present in the laser beam, it can be measured at the rear output, where we take advantage of the monitor photodiode PD2 (see Fig. 1), but also at the front-mirror output. Ideally, we can use a simple beamsplitter (BS) and photodiode PD1 combination to collect it or any equivalent technique to extract some power from the measurement beam.

As demonstrated in [31], the SMI signal in a laser diode (LD) well above threshold is in phase opposition between the two LD outputs. This effect can be exploited to achieve a sort of balanced detection, by taking the difference between PD1 and PD2, as introduced in [32]. Through this difference, all the signal contributions due to LD power variation are canceled, both linked to laser driver noise or disturbances, and also pump current modulations [13], [14], [15], [16].

In this article, we experimentally demonstrate that the balanced detection for SMI is not limited to disturbances reduction but also brings down the optical shot noise contribution, more or less depending on the type of LD.

## II. THEORETICAL MODEL AND ANALYSIS

Let us now start the analysis by evaluating the signals of the front and rear outputs of the LD. Let the power reflectivity of mirrors  $M1$  and  $M2$  be  $R_1$  and  $R_2$ , with output powers  $P_1$  and  $P_2$ . These powers are converted into electrical current signals  $I_1 = \sigma P_1$  and  $I_2 = \sigma P_2$  by photodiodes placed in

Manuscript received 28 March 2023; revised 19 May 2023; accepted 4 June 2023. Date of publication 19 June 2023; date of current version 30 June 2023. The Associate Editor coordinating the review process was Dr. Jae-Ho Han. (*Corresponding author: Michele Norgia.*)

Parisa Esmaili and Michele Norgia are with the Dipartimento di Elettronica, Informazione e Bioingegneria, Politecnico di Milano, I-20133 Milan, Italy (e-mail: parisa.esmaili@polimi.it; michele.norgia@polimi.it).

Silvano Donati is with the Dipartimento di Ingegneria Industriale e Informatica, Università di Pavia, 27100 Pavia, Italy (e-mail: silvano.donati@unipv.it). Digital Object Identifier 10.1109/TIM.2023.3287259

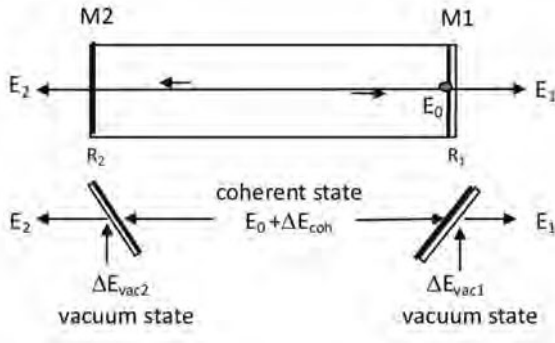


Fig. 2. Second quantization model (bottom) of the LD cavity (top).  $E_0$  is affected by the coherent-state fluctuation  $\Delta E_{\text{coh}}$ , and the vacuum state fluctuations  $\Delta E_{\text{vac}1,2}$  come from the unused ports of the mirrors.

front of the output mirrors. Noise analysis will be carried out in Section III.

Output power  $P$  is a quadratic function of the electric field amplitude  $E$ . The amplitudes of the two output fields  $E_1$  and  $E_2$  have been expressed in [31] as a function of the unperturbed cavity field  $E_0$ , and the parameters of the SMI: target distance  $s$ , attenuation of the back injected field  $A$ , and optical phase shift of the round-trip path to the target  $\phi = 2ks$ , with the wavevector  $k = 2\pi/\lambda$ .

The calculated modulations  $m_1$  and  $m_2$ , defined as the ratio of the SMI signal and the unperturbed field superposed to them, are equal to [27]

$$m_1 = (t_1^2/r_1)(\text{Acos}\phi)[(2\gamma L + \ln R_1 R_2)^{-1} - R_1/T_1] \quad (1)$$

$$m_2 = (t_2^2/r_1)(\text{Acos}\phi)(2\gamma L + \ln R_1 R_2)^{-1}. \quad (2)$$

Hence, the ratio becomes

$$m_1/m_2 = 1 - (R_1/T_1)(2\gamma L + \ln R_1 R_2) \quad (3)$$

where  $r_{1,2} = \sqrt{R_{1,2}}$  and  $t_{1,2} = \sqrt{T_{1,2}}$  are the field reflection and transmission of mirrors  $M1$  and  $M2$ , respectively (see Fig. 2);  $2\gamma L$  is the round-trip gain along the laser cavity of length  $L$ .

As reported in [31], the outputs are in phase ( $m_1/m_2$  close to 1) at small values of the gain minus loss parameter ( $2\gamma L + \ln R_1 R_2$ ); then, in the normal operating conditions for a LD above threshold, with  $2\gamma L + \ln R_1 R_2 > T_1/R_1$ , the outputs become in phase opposition with  $m_1/m_2$  negative, typically  $\approx -0.8$ .

The average components carrying the SMI signals can obviously be brought to the same value by amplification, and in this case, the amplitudes of the two SMI signals measured by PD1 and PD2 are proportional to the modulation coefficients given by (1) and (2).

### III. NOISE ANALYSIS

For a rigorous description of the noise properties of SMI signals, we shall resort to the semi-classical translation of second quantization of the optical field [33]. As shown in Fig. 2, we represent the total field as the superposition of an average  $E_0$  and a fluctuation  $\Delta E_{\text{coh}}$  known as the coherent state fluctuation.  $\Delta E_{\text{coh}}$  is a Gaussian noise, and its amplitude

is such that the power  $P_0 = aE_0^2/2Z_0$  of the field  $E_0$  is the classical shot noise,  $\sigma_p^2 = 2h\nu P_0 B$ , observed on a bandwidth  $B$  [6].  $Z_0$  is the vacuum impedance and  $a$  is the cross section area of the beam.

The fluctuation  $\Delta E_{\text{coh}}$  has zero average,  $\langle \Delta E_{\text{coh}} \rangle = 0$ , and a quadratic mean value given by  $\langle \Delta E_{\text{coh}}^2 \rangle = (a/2Z_0)1/2 h\nu B$  (factor  $a/2Z_0$  is omitted for simplicity in the following). Equivalently,  $\Delta E_{\text{coh}}^2$  has a power spectral density  $d\langle \Delta E_{\text{coh}}^2 \rangle/df = 1/2 h\nu$  equal to half photon per Hertz.

In addition to the noise inherent of the oscillating field, there are other noise sources from BSs and mirrors. Even if any port is unused, indeed, the second quantization theory models it as a port open to the vacuum-state fluctuation,  $\Delta E_{\text{vac}}$  (see Fig. 2). This theory states that the coherent state fluctuation,  $\Delta E_{\text{coh}}$ , is superimposed to every field, and it does not depend on the field amplitude  $E_0$ . It is also present when the amplitude  $E_0 = 0$ , such as in the case of an unused port [29].

Including, as shown in Fig. 2,  $\Delta E_{\text{vac}1}$  and  $\Delta E_{\text{vac}2}$ , the second quantization model is complete [33], and it is possible to evaluate the fluctuations of output fields  $E_1$  and  $E_2$ , and then, the variance of noises superposed to  $P_1$  and  $P_2$ . We will take account of correlation of terms originated by the same fluctuation and of their cancellation in a difference operation, as well as of the uncorrelation of contributions originating by different terms (e.g.,  $\Delta E_{\text{vac}1}$  and  $\Delta E_{\text{vac}2}$ ) that instead will add up.

A preliminary account of the theory, in the special case of equal mirrors reflectivity, has been reported in [34]; here, we develop the general case.

With reference to Fig. 2, we can evaluate the mean value and variance of the power at output 1,  $P_1 = \langle |E_1|^2 \rangle$ . At mirror  $M1$ , we can write

$$E_1 = t_1 (E_0 + \Delta E_{\text{coh}}) + r_1 \Delta E_{\text{vac}1} \quad (4)$$

where  $t_1 = \sqrt{T_1}$  and  $r_1 = \sqrt{R_1}$  are the field transmission and reflection of the mirrors.  $\Delta E_{\text{vac}1}$  has the same distribution, but it is uncorrelated to  $\Delta E_{\text{coh}}$ , entering from the unused port of the BSs. The properties of such fluctuations are

$$\begin{aligned} \langle \Delta E_{\text{coh}} \rangle &= \langle \Delta E_{\text{vac}1} \rangle = 0, \\ \sigma_E^2 &= \langle \Delta E_{\text{coh}}^2 \rangle = \langle \Delta E_{\text{vac}1}^2 \rangle = 1/2h\nu B. \end{aligned} \quad (5)$$

$P_1$  has a mean value given by the classical expression  $\langle P_1 \rangle \propto E^2$ , but we have to subtract the vacuum field, because it cannot be observed, as pointed out in [33]

$$\langle P \rangle_1 = \langle |E_1|^2 \rangle - \langle \Delta E_{\text{vac}1}^2 \rangle. \quad (6)$$

Inserting (4) in (6), we get

$$\begin{aligned} \langle P_1 \rangle &= t_1^2 E_0^2 + t_1^2 \langle \Delta E_{\text{coh}}^2 \rangle + r_1^2 \langle \Delta E_{\text{vac}1}^2 \rangle \\ &+ 2 t_1^2 \langle E_0 \Delta E_{\text{coh}} \rangle + 2 t_1 r_1 \langle E_0 \Delta E_{\text{vac}1} \rangle \\ &+ 2 t_1 r_1 \langle \Delta E_{\text{coh}} \Delta E_{\text{vac}1} \rangle - \langle \Delta E_{\text{vac}1}^2 \rangle. \end{aligned} \quad (7)$$

As the second, third, and last terms cancel out, we obtain

$$\begin{aligned} \langle P_1 \rangle &= t_1^2 E_0^2 + 2 t_1^2 \langle E_0 \Delta E_{\text{coh}} \rangle + 2 t_1 r_1 \langle E_0 \Delta E_{\text{vac}1} \rangle \\ &+ 2 t_1 r_1 \langle \Delta E_{\text{coh}} \Delta E_{\text{vac}1} \rangle. \end{aligned} \quad (8)$$

Also, noting that the mean values of  $\Delta E_{\text{coh}}$  and  $\Delta E_{\text{vac1}}$  are zero,  $E_{\text{coh}}$  and  $E_{\text{vac1}}$  are uncorrelated, and  $E_0^2 = P_0$  and  $t_1^2 = T_1$ , we get

$$\langle P_1 \rangle = t_1^2 E_0^2 = T_1 P_0 \quad (9)$$

that is, the expected result.

Variance is given by the difference  $\sigma_{P_1}^2 = \langle P_1^2 \rangle - \langle P_1 \rangle^2$ , or  $\sigma_{P_1}^2 = t_1^4 E_0^4 + 4 t_1^4 \langle E_0^2 \Delta E_{\text{coh}}^2 \rangle + 4 t_1^2 t_1^2 \langle E_0^2 \Delta E_{\text{vac1}}^2 \rangle - t_1^4 E_0^4 +$  vanishing double products. Substituting  $t_1^2 = T_1$  and  $t_1^2 = R_1$ , we get

$$\sigma_{P_1}^2 = 4T_1^2 E_0^2 \langle \Delta E_{\text{coh}}^2 \rangle + 4T_1 R_1 E_0^2 \langle \Delta E_{\text{vac1}}^2 \rangle. \quad (10)$$

Additionally, as  $T_1 E_0^2 = P_1$  and  $\langle \Delta E_{\text{coh}}^2 \rangle = \langle \Delta E_{\text{vac1}}^2 \rangle = 1/2 h\nu B$ , we finally obtain

$$\sigma_{P_1}^2 = 2T_1 P_1 h\nu B + 2R_1 P_1 h\nu B. \quad (11)$$

Let us note that as  $R_1 + T_1 = 1$ , (11) is also written as  $\sigma_{P_1}^2 = 2P_1 h\nu B$ , corresponding to the variance of power  $P_1$  following a Poisson statistic.

Upon repeating the same calculation for output 2, we get

$$\langle P_2 \rangle = T_2 P_0 = (T_2/T_1) P_1 \quad (12)$$

$$\begin{aligned} \sigma_{P_2}^2 &= 4T_2^2 E_0^2 \langle E_{\text{coh}}^2 \rangle + 4T_2 R_2 E_0^2 \langle E_{\text{vac2}}^2 \rangle \\ &= 2T_2 P_2 h\nu B + 2R_2 P_2 h\nu B. \end{aligned} \quad (13)$$

Before making the difference of SMI signals  $P_1$  and  $P_2$ , we have to equalize their amplitudes, as performed in the experiment's practical implementation by a (noiseless) amplification. For the equalization, in view of (9) and (12), we shall multiply  $P_1$  by  $\sqrt{(T_2/T_1)}$  and  $P_2$  by  $\sqrt{(T_1/T_2)}$ , so that the new mean values become

$$\begin{aligned} \langle P_1 \rangle_{\text{eq}} &= \sqrt{(T_2/T_1)} T_1 P_0 = \sqrt{(T_2 T_1)} P_0 \\ \langle P_2 \rangle_{\text{eq}} &= \sqrt{(T_1/T_2)} T_2 P_0 = \sqrt{(T_2 T_1)} P_0. \end{aligned} \quad (14)$$

As we equalize the mean values, the variances of  $P_1$  and  $P_2$  are multiplied by  $T_2/T_1$  and  $T_1/T_2$ , respectively, so that we have

$$\begin{aligned} \sigma_{P_1}^{2\text{eq}} &= [4T_1^2 E_0^2 \langle E_{\text{coh}}^2 \rangle + 4T_1 R_1 E_0^2 \langle E_{\text{vac1}}^2 \rangle] (T_2/T_1) \\ &= 4T_1 T_2 E_0^2 \langle E_{\text{coh}}^2 \rangle + 4R_1 T_2 E_0^2 \langle E_{\text{vac1}}^2 \rangle \end{aligned} \quad (15)$$

and

$$\begin{aligned} \sigma_{P_2}^{2\text{eq}} &= [4T_2^2 E_0^2 \langle E_{\text{coh}}^2 \rangle + 4T_2 R_2 E_0^2 \langle E_{\text{vac2}}^2 \rangle] (T_1/T_2) \\ &= 4T_1 T_2 E_0^2 \langle E_{\text{coh}}^2 \rangle + 4R_2 T_1 E_0^2 \langle E_{\text{vac2}}^2 \rangle. \end{aligned} \quad (16)$$

Now, comparing (15) and (16), we can see that the first terms of variances are the same, because they derive from the same fluctuation  $E_{\text{coh}}$ . It means that they are canceled out by making the difference  $\Delta P = P_{1\text{eq}} - P_{2\text{eq}}$ . On the contrary, the second terms of (15) and (16) come from different fluctuations,  $E_{\text{vac1}}$  and  $E_{\text{vac2}}$ , and are totally uncorrelated.

Taking this into account, the variance of  $\Delta P = P_{1\text{eq}} - P_{2\text{eq}}$  is written as

$$\begin{aligned} \sigma_{\Delta P}^2 &= 4R_1 T_2 E_0^2 \langle E_{\text{vac1}}^2 \rangle + 4R_2 T_1 E_0^2 \langle E_{\text{vac2}}^2 \rangle \\ &= 4(R_1 T_2 + R_2 T_1) P_0 1/2 h\nu B = 2(R_1 T_2 + R_2 T_1) P_0 h\nu B. \end{aligned} \quad (17)$$

This result must be compared to the variances of the outputs  $P_{1\text{eq}}$  and  $P_{2\text{eq}}$ , which, in view of (15) and (16) and being  $\langle E_{\text{coh}}^2 \rangle = 1/2 h\nu B$ , are given by

$$\sigma_{P_1}^{2\text{eq}} = 4T_2 E_0^2 \langle E_{\text{coh}}^2 \rangle = 2T_2 P_0 h\nu B \quad (18)$$

$$\sigma_{P_2}^{2\text{eq}} = 4T_1 E_0^2 \langle E_{\text{coh}}^2 \rangle = 2T_1 P_0 h\nu B. \quad (18A)$$

Taking the monitor photodiode (rear output,  $P_2$ ) as the reference value, because it is commonly used for self-mixing measurements, we get the ratio of variances equal to

$$\sigma_{\Delta P}^2 / \sigma_{P_2}^{2\text{eq}} = (R_1 T_2 / T_1 + R_2) \quad (19)$$

and the corresponding ratio of SNR, considering also that the differential self-mixing signal has double the amplitude, becomes

$$F = [\text{SNR}_{\Delta P} / \text{SNR}_{P_1}]^2 = 4/[R_1 T_2 / T_1 + R_2]. \quad (20)$$

As a particular case of equal mirrors,  $R_1 = R_2$ , the above equations become

$$\sigma_{\Delta P}^2 = 4 c^2 T R P_0 h\nu B \quad (17')$$

$$\sigma_{P_1}^{2\text{eq}} = \sigma_{P_2}^{2\text{eq}} = 2 c^2 T P_0 h\nu B \quad (18')$$

$$F = 2/R. \quad (20')$$

For a Fabry–Perot (FP) laser, the typical reflectivity is  $R = 0.3$ , corresponding to  $F = 2/0.3 \cong 6.7$ .

If the electronic noise is negligible (in quantum regime [29]), we obtain the same SNR for the output voltage signal  $V = R_{tr} \sigma P$ , given by the photodiode current  $I = \sigma P$ , on a resistance  $R_{tr}$ .

This approach is not applicable to all kinds of lasers, for example, in a He–Ne laser, the two outputs are in phase [31], so the difference cancels out also the useful signal. About previous works, we report that a second-quantization approach was used in [35], for calculating the correlation factors of the two output beams in an FP laser, finding correlation values close to 0.8. With regard to other noise components, in [36], the  $1/f$ -noise correlation was considered, demonstrating an even stronger correlation between the two laser outputs.

In this discussion, we consider amplitude additive noise and its contribution to measurement in the main hypothesis of standard signal processing. For example, small vibration measurement working with the interferometer in quadrature, taking advantage of the signal linearity with target displacement: this is the typical case for evaluating the noise equivalent displacement (NED) of the interferometer [3], [4]. In that condition, phase variation is proportional to amplitude variation; therefore, both noise reduction and signal doubling contribute to improve the measurement. We did not consider phase noise contribution, due to LD limited coherence, because it is typically negligible for short distances.

#### IV. LOW-NOISE PLACEMENT OF THE FRONT PHOTODIODE

Using a BS to pick up power from the front output, as schematically shown in Fig. 1, introduces extra noise, in view of second quantization, because of the unused input port of the BS: it lets the vacuum fluctuation  $E_{\text{vac}}$  enter in the experiment and sum up to the cavity field.

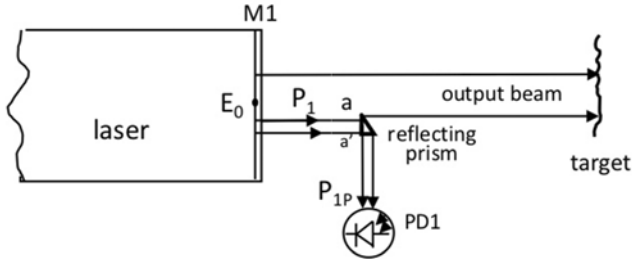


Fig. 3. Using a reflecting prism, to remove a fraction  $a'$  of the output beam, eliminates the vacuum fluctuation of the BS (see Fig. 1).

Indeed, letting  $R_{BS}$  for the BS reflectivity, and following the guidelines of the previous section to calculate powers and associated variances, we find in the case  $R_1 = R_2 = R$  that power at the detector PD1 by is given by

$$P_{1BS} = (r_{BS}t)^2 E_0^2 = R_{BS} P_1 = T R_{BS} P_0 \quad (21)$$

while power at the other mirror is still  $P_1 = t^2 E_0^2 = T P_0$ , a quantity larger than  $P_{1BS}$ . The variance of fluctuations associated with  $P_{1BS}$  is

$$\begin{aligned} \sigma_{P_{1BS}}^2 &= 2T R_{BS} P_{1BS} h\nu B + 2(RR_{BS} + T_{BS}) P_{1BS} h\nu B \\ &= 2TR_{BS}^2 P_1 h\nu B + 2R_{BS}(RR_{BS} + T_{BS}) P_1 h\nu B. \end{aligned} \quad (22)$$

To equalize the amplitude of  $P_{1BS}$  and  $P_2$ , we have to amplify by a factor  $1/R_{BS}$ , getting for the equalized variance  $\sigma_{P_{1BS}(eq)}$

$$\begin{aligned} \sigma_{P_{1BS}(eq)}^2 &= \sigma_{P_{1BS}}^2 / R_{BS}^2 \\ &= \{2TR_{BS}^2 P_1 h\nu B + 2R_{BS}(RR_{BS} + T_{BS}) P_1 h\nu B\} / R_{BS}^2 \\ &= 2TP_1 h\nu B + 2(R + T_{BS}/R_{BS}) P_1 h\nu B \end{aligned} \quad (23)$$

to be compared with

$$\sigma_{P_1}^2 = 2TP_1 h\nu B + 2RP_1 h\nu B..$$

Also, in this case, the first terms are correlated, and the difference becomes

$$\sigma_{\Delta P}^2 = 2(2R + T_{BS}/R_{BS}) P_1 h\nu B \quad (24)$$

and

$$\begin{aligned} \text{SNR}_{\Delta P}^2 &= 4/[2(2R + T_{BS}/R_{BS})](P_1/h\nu B) \\ &= 2/(2R + T_{BS}/R_{BS})(P_1/h\nu B) \end{aligned} \quad (25)$$

whereas the single-channel has  $\text{SNR}_{P_1}^2 = P_1/(2h\nu B)$ .

Thus, the final result is

$$F = [\text{SNR}_{\Delta P}/\text{SNR}_{P_1}]^2 = 2/(R + T_{BS}/2R_{BS}). \quad (26)$$

In conclusion, the insertion of a BS, to take a portion of the emitted light, severely reduces the improvement of the balanced detection. For example, with a 50/50 BS, we have  $F = 2/(R + 1)$ .

In order to overcome this limit, it is more efficient to take a small fraction of the emitted beam by means of a mirror (or a prism, as shown in Fig. 3).

The power collected by PD1 is still a fraction of the emitted power, but in this case, there is no open port to vacuum fluctuations. Indeed, the partialization of the output beam can

TABLE I  
MODEL AND PARAMETERS OF FP, DFB, AND VCSEL LDs

Laser diode Model	structure	$\lambda$ [nm]	$P_o$ [mW]	$I_{th}$ [mA]	$I_{bias}$ [mA]
ADL65052TL	FP	650	5	15	25
HL7851G	FP	785	50	45	80
ML720J11S	DFB	1310	5	6	20
PS85F1P1U-KC	VCSEL	850	0.5	2	5

be modeled as a two-port device, instead of the four port of the BS.

Therefore, expression (11) also holds for this setup, with  $P_1$  replaced by  $P_{1P}$ , and the improvement in SNR is confirmed.

Another possible solution is placing the external photodiode directly to detect a fraction of the output beam. This solution allows to minimize part count and cost, and it is particularly indicated when the monitor photodiode intercepts a small fraction of the emitted power (a very common situation for visible and near-infrared LDs).

## V. EXPERIMENTS

The purpose of this section is the experimental verification of the improvement obtainable through the balanced configuration of SMI in terms of SNR. As demonstrated in Section III, the achievable improvement depends on the reflectivity of the laser mirrors; therefore, it is expected to obtain different results depending on the type of laser tested. In this article, two different FP LDs, one distributed-feedback (DFB), and one vertical-cavity surface-emitting (VCSEL) LD have been tested. Table I reports LDs models with their main specifications: wavelength ( $\lambda$ ), output power ( $P_o$ ), threshold current ( $I_{th}$ ), and biased dc current ( $I_{bias}$ ).

For the verification, a special power supply and measurement electronics was developed, capable of switching from a single-PD configuration to a balanced configuration by acting on simple jumpers. Fig. 4 shows a simplified circuit diagram of the LD driver and transimpedance amplifier, realized for implementing the subtraction between internal and external photodiodes. As shown in this figure, both monitor and external photodiodes are fed to the same trans-impedance amplifier with a 100-k $\Omega$  feedback resistor. The output signal of the transimpedance amplifier is proportional to  $\Delta P = P_1 - P_2$  which is directly connected to a digital oscilloscope (model RTB2004). The employed external photodiodes are: a silicon photodiode (model BPW34) with a spectral range of 430–1100 nm and an InGaAs photodiode (model SD039-151-011) with a spectral range of 800–1700 nm. For balancing  $P_1$  and  $P_2$ , a 16-kHz triangular waveform with an amplitude of 1.5 mA is applied as a modulation signal to the LD bias current. The external photodiode is mounted on a slider to adjust its position for canceling the current modulation measured in transimpedance output, proportional to  $\Delta P$ . Once the equal amplitude condition is satisfied, the modulation signal can be easily removed using a jumper (J3 in Fig. 4). To evaluate the self-mixing signal, the laser beam is focused on white article, placed on a loudspeaker at about 10 cm from the LD, using a biconvex lens with a focal length of 25 mm. Fig. 5 shows a

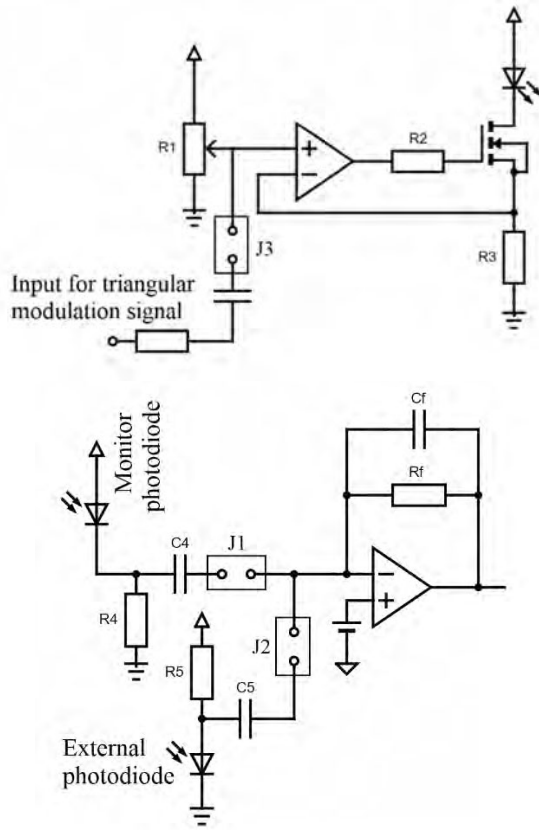


Fig. 4. Simplified circuit diagram of the driver (top) and readout circuitry for balance detection (bottom).

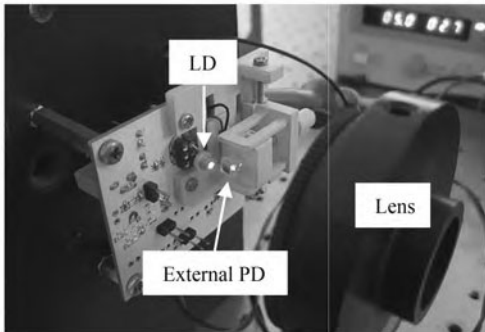


Fig. 5. Photograph of the experimental setup.

photograph of the experimental setup. For noise measurement, the target is removed in order to avoid spurious SMI signals.

## VI. RESULTS AND DISCUSSION

For every tested LD, after the balancing of the power measured by external and monitor PD, we acquired the transimpedance output, with and without the external photodiode, by acting on jumper J2 (see Fig. 4). Great care was taken to avoid any possible change in mechanical alignment or physical condition and to minimize electrical disturbances on LD supply, because as already demonstrated in [32], they cancel out in balanced detection and may appear to have a more marked improvement in SNR. The power spectrum in dBm is directly calculated by the digital oscilloscope, considering

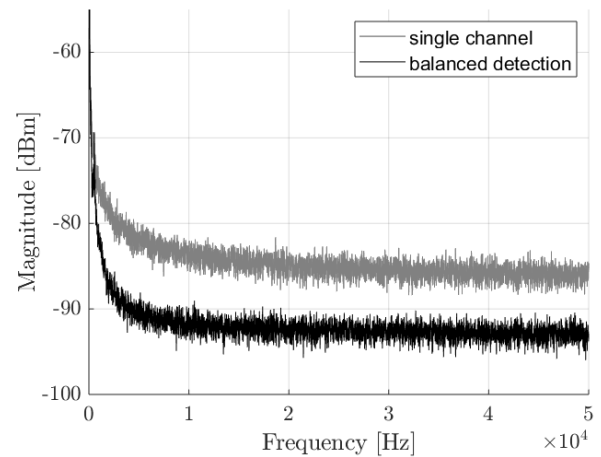


Fig. 6. Power spectrum of the voltage signal at the transimpedance amplifier output, for ADL65052TL: single channel (upper trace) and balanced detection (lower trace).

50- $\Omega$  load. With the same mechanical setup, a vibrating target is added to evaluate SMI signal with and without the external photodiode.

Self-mixing signal amplitude decreases with temperature, as shown in [37]. In this work, we did not consider that dependence and we made all the comparisons at the same temperature.

The first tested LD is a very-common FP red laser. This laser is often used for the demonstration of the SMI signal, because it is low cost, easy to find, and quite sensitive to optical back injection, even if it is not robust to moderate feedback level. Fig. 6 shows the power spectrum comparison: with both PDs connected (balanced detection) and with only monitor PD (single channel). In this case, the noise reduction is evident, about 6 dB, and can be appreciated also in the time-domain SMI signal (see Fig. 7). Here, we get about 12 dB of SNR improvement, considering the signal doubling, also evident in Fig. 7. This improvement is coherent with the theory of Section III, if considering the anti-reflection coating of the LD output facet, very common for red LD [38]. Indeed, (20) gives about 11 dB of SNR improvement for 1%–2% output mirror reflectivity.

The second tested laser is one of the most employed LDs for SMI interferometer [6], [7], [14], because of its very-good sensitivity and robustness to back injection: near-infrared FP LD, model HL7851G. For this LD, the noise reduction is exactly what is expected from theory: for cleaved facets ( $R = 0.3$ ), it is about 2 dB (see Fig. 8). As shown in Fig. 9, the signal doubling leads to about 8 dB of SNR improvement for this laser.

It is worth noting that the monitor PD takes a small fraction of the emitted power (about 1%, typical for this kind of LD); therefore, it is easy to place the external photodiode without excessively choking the SMI measurement beam.

Next tested LD is a DFB model, also often used for SMI [8], [17], [37], [39]. The distributed feedback is not perfectly modeled by the proposed theory, but we can evaluate experimental results and consider a sort of equivalent mirror reflectivity. In

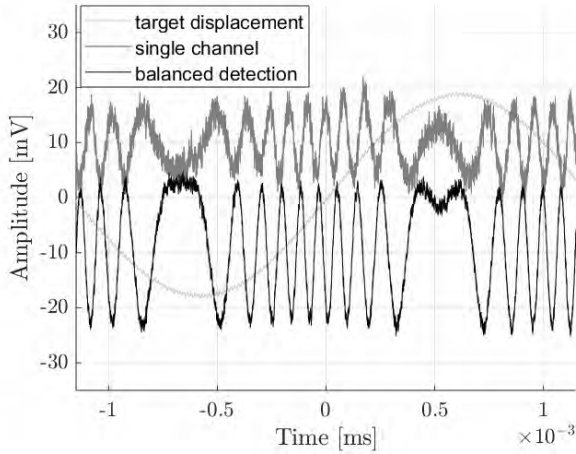


Fig. 7. Interferometric self-mixing signal waveforms using ADL65052TL: single channel (upper trace) and balanced detection (lower trace).

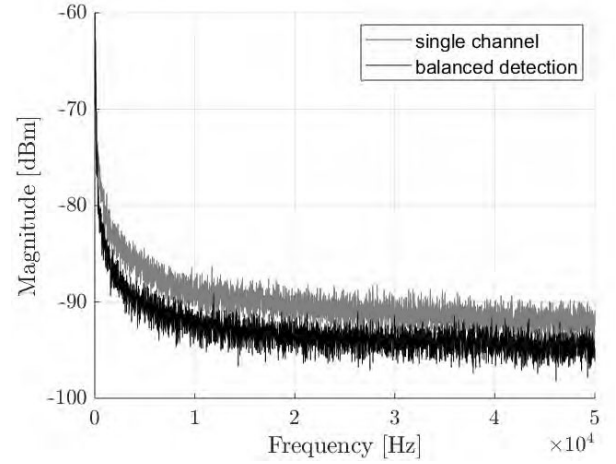


Fig. 10. Power spectrum of the voltage signal at the transimpedance amplifier output for ML720J11S: single channel (upper trace) and balanced detection (lower trace).

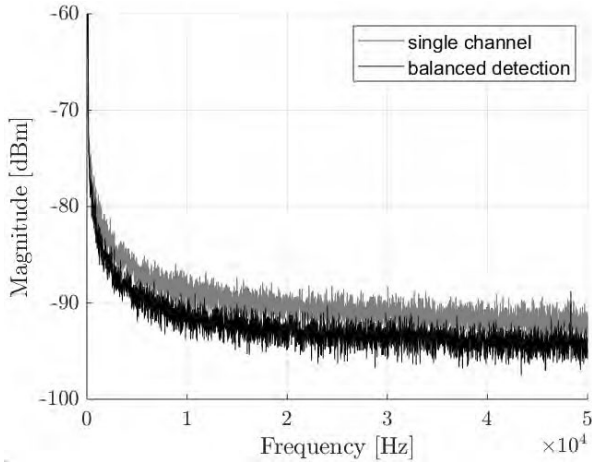


Fig. 8. Power spectrum of the voltage signal at the transimpedance amplifier output, for HL7851G: single channel (upper trace) and balanced detection (lower trace).

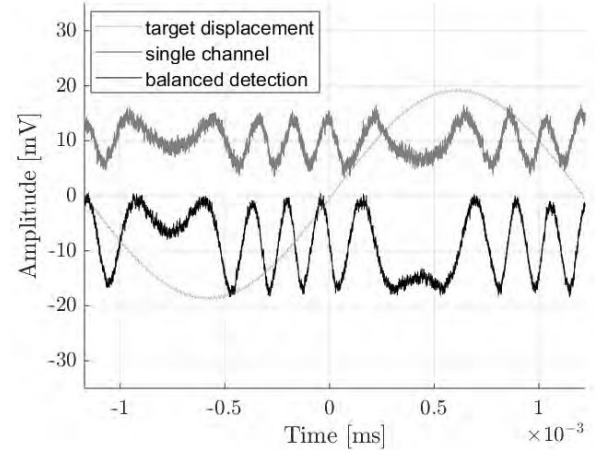


Fig. 11. Interferometric self-mixing signal waveforms using ML720J11S: single channel (upper trace) and balanced detection (lower trace).

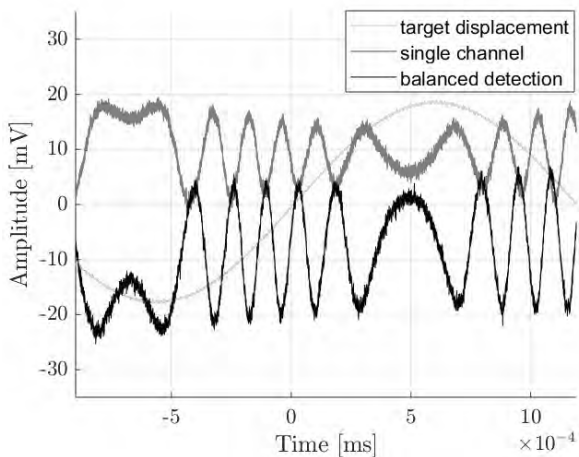


Fig. 9. Interferometric self-mixing signal waveforms using HL7851G: single channel (upper trace) and balanced detection (lower trace).

this case, noise reduction is similar to the FP laser without reflection coating, about 2 dB for shot noise contribution, as shown in Fig. 10 (for frequency higher than 30 kHz). It

is a little higher for  $1/f$  noise, about 4 dB. This behavior is not explained by the proposed theory, but it is already known that shot-noise and  $1/f$  noise can have different correlations between the two LD outputs [36]. Even the SNR improvement is similar to the one for HL7851G, considering that we still have a doubling in the SMI signal (see Fig. 11).

The last LD model considered is a single-mode VCSEL, with an internal monitor photodiode. Fig. 12 shows the noise spectrum with and without the external photodiode. In this case, the difference is negligible ( $\sim 0$  dB). This indicates that there is a slight correlation; otherwise, it would be +3dB, but it is lower than the other LDs tested. From (20), this value suggests equivalent mirrors reflectivity of about 50%. Fig. 13 reports the time-domain SMI signals, showing an amplitude improvement of only  $\sim 50\%$  from the subtraction, as predicted by (5).

Table II summarizes the experimental results for the different LDs. As evident in the time-domain signals, a strong improvement is obtained for low-cost red LD, while for the VCSEL, the advantages of the proposed technique are negligible with respect to the additional complexity.

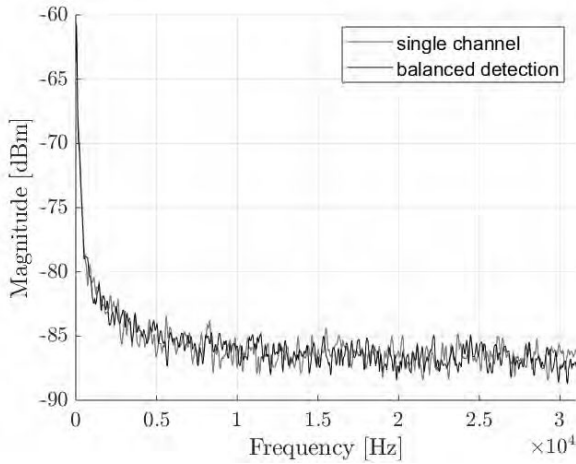


Fig. 12. Power spectrum of the voltage signal at the transimpedance amplifier output for PS85F1P1U: single channel (upper trace) and balanced detection (lower trace).

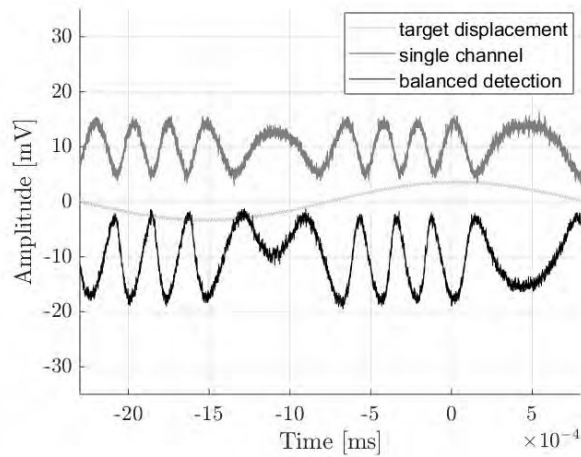


Fig. 13. Interferometric self-mixing signal waveforms photodiode using PS85F1P1U-KC: single channel (upper trace) and balanced detection (lower trace).

TABLE II

TOTAL SNR IMPROVEMENT FOR FP, DFB, AND VCSEL LDs

Laser diode Model	SNR improvement due to signal opposition [dB]	SNR improvement due to partially correlated noise fluctuation [dB]	Total SNR Improvement [dB]
ADL65052TL	6	~6	~12
HL7851G	6	~2	~8
ML720J11S	6	~2	~8
PS85F1P1U-KC	3	~0	~3

## VII. CONCLUSION

In this article, we confirmed experimentally a rigorous theory based on second quantization developed to evaluate the signal-to-noise improvement of the balanced detector configuration used in an SMI. We have tested several specimens of LDs and found excellent agreement between theoretical and experimental values. In particular, we have shown that an improvement of up to 12 dB can be obtained in SNR of a self-mixing measurement with a red FP LD.

Another important finding is about the placement of the front-exit pickup of signal: both theory and experiment show

that it should be done by partializing the beam rather than by an ordinary BS because the latter opens a port on the vacuum fluctuations.

The results obtained are relevant to several applications of SMI, like, for example, absolute distance measurement [15] vibration sensing, and all the measurements involving a small amplitude of returning signal [9], [10].

## REFERENCES

- [1] S. Donati, "Developing self-mixing interferometry for instrumentation and measurements," *Laser Photon. Rev.*, vol. 6, no. 3, pp. 393–417, May 2012.
- [2] T. Taimre, M. Nolic, K. Bertling, Y. L. Lim, T. Bosch, and A. D. Rakic, "Laser feedback interferometry: A tutorial on the self-mixing effect for coherent sensing," *Adv. Opt. Photon.*, vol. 7, no. 3, pp. 570–631, 2015.
- [3] G. Giuliani, M. Norgia, S. Donati, and T. Bosch, "Laser diode self-mixing technique for sensing applications," *J. Opt. A, Pure Appl. Opt.*, vol. 4, no. 6, pp. S283–S294, Nov. 2002.
- [4] S. Donati, *Electro-Optical Instrumentation—Sensing and Measuring With Lasers*. Upper Saddle River, NJ, USA: Prentice-Hall, 2004.
- [5] S. Donati and M. Norgia, "Overview of self-mixing interferometer applications to mechanical engineering," *Opt. Eng.*, vol. 57, no. 5, p. 1, Mar. 2018, doi: 10.1117/1.OE.57.5.051506.
- [6] C. Bes, G. Plantier, and T. Bosch, "Displacement measurements using a self-mixing laser diode under moderate feedback," *IEEE Trans. Instrum. Meas.*, vol. 55, no. 4, pp. 1101–1105, Aug. 2006, doi: 10.1109/TIM.2006.876544.
- [7] A. Magnani, A. Pesatori, and M. Norgia, "Real-time self-mixing interferometer for long distances," *IEEE Trans. Instrum. Meas.*, vol. 63, no. 7, pp. 1804–1809, Jul. 2014, doi: 10.1109/TIM.2013.2297816.
- [8] S. Ottonelli, F. De Lucia, M. di Vietro, M. Dabbicco, G. Scamarcio, and F. P. Mezzapesa, "A compact three degrees-of-freedom motion sensor based on the laser-self-mixing effect," *IEEE Photon. Technol. Lett.*, vol. 20, no. 16, pp. 1360–1362, Aug. 15, 2008, doi: 10.1109/LPT.2008.926569.
- [9] M. Norgia and S. Donati, "A displacement-measuring instrument utilizing self-mixing interferometry," *IEEE Trans. Instrum. Meas.*, vol. 52, no. 6, pp. 1765–1770, Dec. 2003, doi: 10.1109/TIM.2003.820451.
- [10] H. Wang, Y. Ruan, Y. Yu, Q. Guo, J. Xi, and J. Tong, "A new algorithm for displacement measurement using self-mixing interferometry with modulated injection current," *IEEE Access*, vol. 8, pp. 123253–123261, 2020, doi: 10.1109/ACCESS.2020.3007516.
- [11] S. Donati, R. Gotti, A. Agnesi, and F. Pirzio, "Self-mixing displacement measured by a two-color laser in 66-nm steps," *IEEE Trans. Instrum. Meas.*, vol. 72, pp. 1–7, 2023, doi: 10.1109/TIM.2022.3227611.
- [12] S. S. Khurshid, W. Hussain, U. Zabit, and O. D. Bernal, "Augmentation-assisted robust fringe detection on unseen experimental signals applied to optical feedback interferometry using a deep network," *IEEE Trans. Instrum. Meas.*, vol. 72, pp. 1–10, 2023, doi: 10.1109/TIM.2023.3251409.
- [13] T. Bosch, N. Servagent, R. Chellali, and M. Lescure, "Three-dimensional object construction using a self-mixing type scanning laser range finder," *IEEE Trans. Instrum. Meas.*, vol. 47, no. 5, pp. 1326–1329, Jan. 1998.
- [14] M. Norgia, D. Melchionni, and A. Pesatori, "Self-mixing instrument for simultaneous distance and speed measurement," *Opt. Lasers Eng.*, vol. 99, pp. 31–38, Dec. 2017.
- [15] F. Cavedo, P. Esmaili, and M. Norgia, "Self-mixing laser distance-sensor enhanced by multiple modulation waveforms," *Sensors*, vol. 22, no. 21, p. 8456, Nov. 2022, doi: 10.3390/s22218456.
- [16] L. Rovati, L. D. Cecilia, and S. Cattini, "On the feasibility of absolute distance measurement by using optical feedback into a superluminescent diode cavity," *IEEE Trans. Instrum. Meas.*, vol. 69, no. 5, pp. 2495–2506, May 2020, doi: 10.1109/TIM.2019.2956421.
- [17] Z. A. Khan, U. Zabit, O. D. Bernal, M. O. Ullah, and T. Bosch, "Adaptive cancellation of parasitic vibrations affecting a self-mixing interferometric laser sensor," *IEEE Trans. Instrum. Meas.*, vol. 66, no. 2, pp. 332–339, Feb. 2017, doi: 10.1109/TIM.2016.2626018.
- [18] R. Li et al., "All-fiber laser-self-mixing interferometer with adjustable injection intensity for remote sensing of 40 km," *J. Lightw. Technol.*, vol. 40, no. 14, pp. 4863–4870, Jul. 15, 2022, doi: 10.1109/JLT.2022.3170459.

- [19] B. Liu, Y. Ruan, and Y. Yu, "All-fiber laser-self-mixing sensor for acoustic emission measurement," *J. Lightw. Technol.*, vol. 39, no. 12, pp. 4062–4068, Jun. 15, 2021.
- [20] A. Magnani, D. Melchionni, A. Pesatori, and M. Norgia, "Self-mixing digital closed-loop vibrometer for high accuracy vibration measurements," *Opt. Commun.*, vol. 365, pp. 133–139, Apr. 2016, doi: 10.1016/j.optcom.2015.12.002.
- [21] M. Norgia, A. Pesatori, and S. Donati, "Compact laser-diode instrument for flow measurement," *IEEE Trans. Instrum. Meas.*, vol. 65, no. 6, pp. 1478–1483, Jun. 2016, doi: 10.1109/TIM.2016.2526759.
- [22] R. Atashkooei, E. E. Ramírez-Miquet, R. D. C. Moreira, A. Quotb, S. Royo, and J. Perchoux, "Optical feedback flowmetry: Impact of particle concentration on the signal processing method," *IEEE Sensors J.*, vol. 18, no. 4, pp. 1457–1463, Feb. 2018, doi: 10.1109/JSEN.2017.2781902.
- [23] M. Norgia, A. Pesatori, and L. Rovati, "Low-cost optical flowmeter with analog front-end electronics for blood extracorporeal circulators," *IEEE Trans. Instrum. Meas.*, vol. 59, no. 5, pp. 1233–1239, May 2010, doi: 10.1109/TIM.2009.2038015.
- [24] H. Liang et al., "Wearable and multifunctional self-mixing microfiber sensor for human health monitoring," *IEEE Sensors J.*, vol. 23, no. 3, pp. 2122–2127, Feb. 2023, doi: 10.1109/JSEN.2022.3225196.
- [25] I. Milesi, M. Norgia, P. P. Pompilio, C. Svelto, and R. L. Dellaca, "Measurement of local chest wall displacement by a custom self-mixing laser interferometer," *IEEE Trans. Instrum. Meas.*, vol. 60, no. 8, pp. 2894–2901, Aug. 2011, doi: 10.1109/TIM.2011.2118830.
- [26] S. Donati and M. Norgia, "Self-mixing interferometry for biomedical signals sensing," *IEEE J. Sel. Topics Quantum Electron.*, vol. 20, no. 2, pp. 104–111, Mar. 2014, doi: 10.1109/JSTQE.2013.2270279.
- [27] V. Contreras, J. Lonngqvist, and J. Toivonen, "Edge filter enhanced self-mixing interferometry," *Opt. Lett.*, vol. 40, no. 12, p. 2814, Jun. 2015.
- [28] M. Norgia, D. Melchionni, and S. Donati, "Exploiting the FM-signal in a laser-diode SMI by means of a Mach-Zehnder filter," *IEEE Photon. Techn. Lett.*, vol. 29, no. 18, pp. 1552–1555, Aug. 3, 2017, doi: 10.1109/LPT.2017.2735899.
- [29] S. Donati and M. Norgia, "Self-mixing interferometer with a laser diode: Unveiling the FM channel and its advantages respect to the AM channel," *IEEE J. Quantum Electron.*, vol. 53, no. 5, pp. 1–10, Oct. 2017.
- [30] M. Norgia, V. Contreras, and S. Donati, "Noise in an FM-converted self-mixing interferometer," *IEEE Trans. Instrum. Meas.*, vol. 69, no. 7, pp. 5100–5106, Jul. 2020, doi: 10.1109/TIM.2019.2957867.
- [31] E. M. Randone and S. Donati, "Self-mixing interferometer: Analysis of the output signals," *Opt. Exp.*, vol. 14, no. 20, pp. 9788–9796, 2006.
- [32] K. Li, F. Cavedo, A. Pesatori, C. Zhao, and M. Norgia, "Balanced detection for self-mixing interferometry," *Opt. Lett.*, vol. 42, no. 2, pp. 283–285, 2017.
- [33] S. Donati, *Photodetectors—Devices, Circuits and Applications*, 2nd ed. Hoboken, NJ, USA: Wiley, 2021, pp. 427–432.
- [34] S. Donati and M. Norgia, "SNR improvement of 8.2 dB in a self-mixing laser diode interferometer by using the difference signal at the output mirrors," *Chin. Opt. Lett.*, vol. 19, no. 9, 2021, Art. no. 092502.
- [35] J.-L. Vey, A. Karsten, K. Auen, and W. Elsässer, "Intensity fluctuation correlation for a Fabry Perot semiconductor laser: A semiclassical analysis," *Opt. Commun.*, vol. 146, nos. 1–6, pp. 325–338, Jan. 1998.
- [36] R. J. Fronen, "Correlation between 1/f fluctuations in the two output beams of a laser diode," *IEEE J. Quantum Electron.*, vol. 27, no. 4, pp. 931–936, Apr. 1991.
- [37] J. A. Roumy et al., "Effect of injection current and temperature on signal strength in a laser diode optical feedback interferometer," *Appl. Opt.*, vol. 54, no. 2, pp. 312–318, 2015, doi: 10.1364/AO.54.000312.
- [38] C. Z. Kim, J. H. Choi, C. S. Shin, and H. Kim, "Effect of antireflection facet coatings on the characteristics of a high-power red laser diode," *J. Korean Phys. Soc.*, vol. 64, no. 10, pp. 1421–1424, May 2014.
- [39] S. Donati and M. Norgia, "Native signal self-mix interferometer has less than 1 nm noise equivalent displacement," *Opt. Lett.*, vol. 46, pp. 1995–1998, Jan. 2021.



**Parisa Esmaili** was born in Marand, Iran, in 1988. She received the B.S. degree in electronics engineering from Azad University, Urmia, Iran, in 2011, the M.S. degree in electrical engineering from University Technology Malaysia (UTM), Johor Bahru, Malaysia, in 2014, and the Ph.D. degree in electrical engineering from Politecnico di Milano, Milan, Italy, in 2020.

She is currently an RTDA Researcher at Politecnico di Milano. Her main research interests include electrical, optical, and biomedical measurement and instrumentation, signal processing, and soft computing methods.



**Michele Norgia** (Senior Member, IEEE) was born in Omegna, Italy, in 1972. He received the M.S. degree (Hons.) in electronics engineering and the Ph.D. degree in electronics engineering and computer science from the University of Pavia, Pavia, Italy, in 1996 and 2000, respectively.

In 2006, he joined the Department of Electronic and Information Science, Politecnico di Milano, Milan, Italy, as an Assistant Professor of electric and electronic measurements. Since 2016, he has been a Full Professor of electronic measurements.

He is the author of more than 250 articles published in international journals or conference proceedings. His main research interests include optical and electronic measurements, interferometry, chaos in lasers, optical frequency standards, microelectromechanical sensors, biomedical measurements, and instrumentation.

Prof. Norgia is the member of the Italian Association "Group of Electrical and Electronic Measurements."



**Silvano Donati** (Life Fellow, IEEE) received the Ph.D. degree (cum laude) in physics from the University of Milan, Milan, Italy, in 1966.

He has been a Full Professor with the University of Pavia, Pavia, Italy, since 1980, before becoming Emeritus, in 2015. He has authored or coauthored 350+ articles and holds a dozen patents and has written two books, "Photodetectors" (1st ed.: Prentice Hall, 2000; 2nd ed.: IEEE, Wiley 2021) and "Electro-Optical Instrumentation" (1st ed.: Prentice Hall 2004; 2nd ed.: CRC 2023), covering the subject

of his courses at the University of Pavia and abroad. His main achievements have been self-mixing interferometry and chaos-shift-keying cryptography, the topics covered in his Distinguished Lecture talk given in 21 LEOS (now IPS) Chapters in two terms (2007–2009) and continued as a Traveling Lecturer of OSA and SPIE on Self-Mixing and Lidars to date, covering a total 105 Chapters visited.

Dr. Donati is a Optica Emeritus Fellow and SPIE Life Member. He has received several awards from the AEIT and IEEE, in particular, the Marconi medal, the Aaron Kressel Award, and the Distinguished Service Award of the IEEE Photonics Society. He was the founder (1996) and first Chairman (1997–2001) of the Italian LEOS Chapter, LEOS VP Region 8 Membership (2002–2004) and BoG (2004–2006), and the Chairman of the IEEE Italy Section (2008–2009). He has spent semesters as a Visiting Professor in several Universities of Taiwan: NTU in Taipei, 2005, Sun Yat Sen in Kaohsiung (2007, 2008, 2010), NCKU in Tainan, 2012, NCHU in Taichung, 2013–2014, NTUT in Taipei 2015–2016, and NTU in Taipei 2018–2019. He is also an Associate of the Italian Institute of Optics (ISASI) of the National Science Foundation (CNR).